Acoustic monitoring of compaction in cohesive granular materials

Vincent Canel,[1,2] Xiaoping Jia,[1,*] Michel Campillo,[2] and Ioan Ionescu[3]
[1]*Institut Langevin, ESPCI Paris, Université PSL, CNRS, Paris 75005, France*
[2]*ISTerre, CNRS, UMR 5275, Université Grenoble Alpes, 38000 Grenoble, France*
[3]*LSPM, CNRS UPR 3407, Université Paris 13, 93430 Villetaneuse, France*

(Received 3 November 2023; accepted 16 January 2024; published 12 February 2024)

We study the transition from cohesive to noncohesive states of cemented granular materials (synthetic rocks) under oedometric loading, combining simultaneous measurements of ultrasound velocity and acoustic emission (AE: microseosmicity). Our samples are agglomerates made of glass beads bonded with a few percent of cement, either ductile or brittle. These cemented granular samples exhibit an inelastic compaction beyond certain axial stresses likely due to the formation of compaction bands, which is accompanied by a significant decrease of compressional wave velocity. Upon subsequent cyclic unloading-reloading with constant consolidation stress, we found the mechanical and acoustic responses like those in noncohesive granular materials, which can be interpreted within the effective medium theory based on the Digby's bonding model. Moreover, this model allows P-wave velocity measured at vanishing pressure to be interpreted as an indicator of the debonding on the scale of grain contact. During the inelastic compaction, stick-slip-like stress drops were observed in brittle cement-bonded granular samples accompanied by the instantaneous decrease of the P-wave velocity and AEs which display an Omori-like law for foreshocks, i.e., precursors. By contrast, mechanical responses of ductile cement-bonded granular samples are smooth (without visible stick-slip-like stress drops) and mostly aseismic. By applying a cyclic loading-unloading with increasing consolidation stress, we observed a Kaiser-like memory effect in the brittle cement-bonded sample in the weakly damaged state which tends to disappear when the bonds are mostly broken in the noncohesive granular state after large-amplitude loading. In this paper, we show that the macroscopic ductile and brittle behavior of cemented granular media is controlled by the local processes on the scale of the bonds between grains.

DOI: 10.1103/PhysRevE.109.024902

I. INTRODUCTION

Deformation of rocks involves damage processes such as microcrack nucleation and propagation. During the deformation process, damage localization can lead to the creation of macroscopic fractures (e.g., shear bands) and to the failure of the material associated with a dramatic decrease of its strength and modulus. The damage activity may also be investigated through the seismic activity emitted by crack propagation, i.e., acoustic emission (AE). On the geological scale, earthquakes or fault core sliding occur naturally in response to long-term deformation produced by plate tectonics. However, the way the damage and the cohesiveness of the damaged rocks control the frictional slip and the seismic patterns is not well understood [1]. Indeed, typical faults consist of a narrow fault core of almost purely granular material, where earthquake slip localizes [2], surrounded by a fractured crust (off-fault damage zone) whose fracture density decreases with distance away from the fault core [3,4].

On the laboratory sample scale, a similar behavior can be reproduced through triaxial loading experiments on initially fractured rocks (e.g., containing a sawcut), a likely situation in a preexisting seismic fault [5]. According to observations, stable sliding or stick-slip instabilities depend on loading conditions, well rationalized by the rate and state friction law [6,7]. However, for initially unfractured rocks, two distinct mechanical responses and failure modes are observed [8]. For brittle materials, the failure occurs due to the cooperative interaction of local (micro)ruptures, i.e., damage localized into a narrow shear band (inclined at 30°–45° compared with the compressive load direction) as loading proceeds, that can be dynamically observed by AE and source localization (cracking noise). Ductile behavior associated with diffuse damage (macroscopic plasticity) can also be observed for the same materials by increasing the confining pressure. In both cases, AE event distributions exhibit power-law behavior pointing to long-range correlations; nevertheless, their behaviors appear to be akin respectively to the first-order and critical phase transitions [1,9]. These observations are confirmed by various numerical models and simulations [10–12].

In addition to the formation of shear bands, compaction bands have also been observed in porous (granular) sandstones at a critical confining (hydrostatic) pressure, monitored by the AE source location detections and the elastic wave velocities evolution. They are localized compressive deformation zones mostly perpendicular to the main stress direction due to grain crushing and pore collapse [13–15]. If the increase of local density under load results in strengthening, formation of a compaction band may not preclude later

*xiaoping.jia@espci.fr

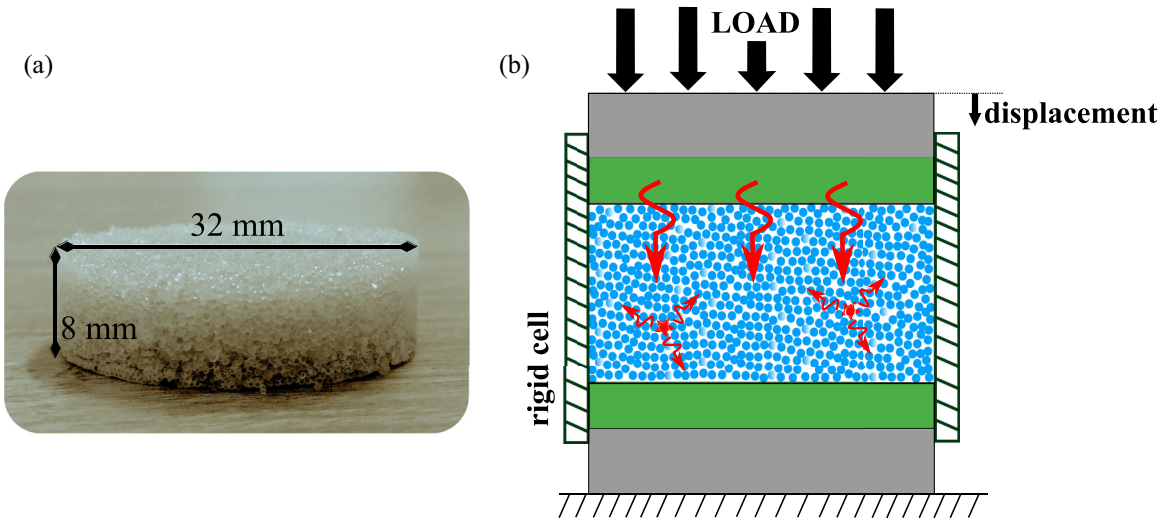

FIG. 1. (a) The cemented granular material is placed between two ultrasonic transducers (sketched in green) in a rigid cell closed by two pistons, (b) i.e., oedometric testing. The upper piston transmits the load through a controlled displacement (axial strain-driven). The active acoustic probing is conducted with the source ultrasonic transducer (top) transmitting a short pulse (long red arrows) and the detector (bottom), while the passive detection, i.e., acoustic emissions (red stars) are recorded by the ultrasonic detector.

formation of a shear band or failure [16]. Such inelastic compaction and associated porosity reduction play an important role in the diagenesis of sandstone and may affect the reservoir stability during hydrocarbon production.

In this paper, we focus our investigation on the damage process during inelastic compaction. To this end, we perform controlled laboratory experiments on cohesive granular materials under oedometric loading for which shear banding is likely excluded. Our synthetic rocks are made of glass beads bonded with a few percent of cement, either ductile or brittle. Compared with previous works [17,18], here, we acoustically monitor the damage and fracture process by measuring both the change in compressional wave velocity (active source) [19] and the AE (microseismicity), if any [20]. Our aim is twofold. First, unlike porous sandstones, the inelastic compaction considered here shall be associated with the debonding instead of grain crushing [12,21]. These cemented granular materials allow a close comparison between experiments and theory based on the Digby granular model. By measuring the compressional wave velocity at vanishing confining pressure, this model provides a qualitative indicator of the bond damage-breakage induced by cyclic loading-unloading from (continuum) cemented state to (discrete) granular state [22]. Secondly, by controlling the local interaction and damage process through ductile- and brittle-cement-bonded glass beads, we seek a possible link with the associated ductile and brittle behaviors on the macroscopic scale.

In the following sections, we first describe the preparation protocol of cemented granular samples (Sec. II A) and combined oedometric tests, ultrasonic measurements, and AE detections in these materials, under constant (Sec. II B) and increasing (Sec. II C) consolidation stresses, respectively. In Sec. III, we analyze the compressional wave velocity and damage process within the effective medium framework based on a heuristic bonded contact (Secs. III A and III B). We also discuss the Omori-like behavior and the memory effect (Kaiser effect) with AE analysis at constant and increasing consolidation stresses (Sec. III C).

II. EXPERIMENTS

A. Sample preparation and oedometric loading

Our cemented granular materials are composed of polydisperse glass beads of diameter $d = 400$–800 μm bonded with either ductile or brittle cement. The packing fraction of the beads is $\phi_s \approx 60\%$, and the cement volume fraction $\phi_c \approx 1.5\%$ (compared with the total volume of the samples). One of the cylindrical samples is shown in Fig. 1(a), with diameter $D = 32$ mm and thickness $e_0 = 8.0$ mm. The ductile cement is made of eicosane that tolerates large deformation before breakage, while the brittle cement is salol that breaks readily under stress. The cement powders are added to glass beads in a cylindrical mold and then placed into an oven at a temperature just greater than the melting point of the cement ($\sim 40\,^\circ$C). Once the cement is melted after a few minutes of heating, we stir the mixture to distribute evenly the cement with the beads. The mixture is then closed in the mold and submitted to cycles of oedometric loadings and unloading that allow us to compact the sample before the cooling and solidification of the cement at room temperature.

Once cooled, cemented granular samples are placed into a cylindrical oedometric cell of the same diameter. Two large longitudinal broadband transducers (of diameter $D = 32$ mm) are put in contact with the sample as pistons [in green, Fig. 1(b)]. They transmit the load to the sample from a uniaxial electromechanical press, under a controlled displacement speed (i.e., axial strain driven), monotonic or cyclic. For the range of axial loading force F applied here, we have verified that the beads remain intact (not crushed) after the test. Acoustic measurements are performed during the external loading to monitor the damage process of the sample under compression.

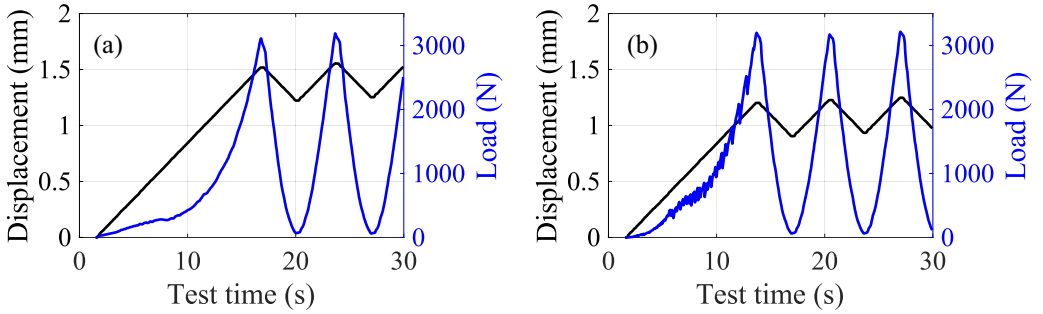

FIG. 2. Both displacement and force are measured as a function of the test time at an imposed loading speed (strain-driven) with the (a) ductile-cement and (b) brittle-cement bonded granular samples.

B. Damage evolution under cyclic loading with constant consolidation stress

1. Mechanical response

Figure 2 depicts the displacements (black curves) and forces (blue ones) measured, respectively, as a function of the test time in the ductile-cement-bonded [Fig. 2(b)] and brittle-cement-bonded granular samples [Fig. 2(b)]. In this uniaxial testing, the loading speeds are imposed at 100 μm/s (strain driven), as illustrated in Figs. 2(a) and 2(b) by the constant slopes in the linear displacement-time responses, for the first loading and successive reloading (after unloading). When the load reaches the maximum amplitude $F = 3000$ N [corresponding to an axial stress of $P = F/(\pi D^2) \approx 3.7$ MPa], the sample is unloaded to $F = 60$ N ($P \approx 75$ kPa) and then submitted to a dozen cycles of unloading-loading between 60 and 3000 N. A nonzero unload lower limit was used to keep the contact between transducers and the granular sample for ensuring reproducible measurements.

Figure 3 shows the cross-plots of the loading force as a function of the displacement in the ductile- and brittle-cement-bonded granular samples. For the ductile-cement-bonded sample [Fig. 3(a)], the load first increases linearly with the displacement from A to B then deviates nonlinearly from B to E, pointing to plastic deformations. More specifically, we observed the appearance of a plateau in the load-displacement curve from C to D for numerous tests with different cemented samples. It suggests the growth of microscopic cracks (initiated at point B) into mesoscopic or macroscopic fractures in cemented samples, leading to a plastic deformation on the macroscopic or sample scale. Mechanical responses are fundamentally different between the first loading and subsequent unloading-reloading cycles. The latter is reminiscent of the behavior observed in noncohesive, dry granular materials (unconsolidated), where small hysteretic loops are detected between the loading and unloading paths. They are accompanied by a slight compaction [23] and tend to an almost stationary narrow loop, displaying a Hertzian-like force-displacement relationship [24].

For the brittle-cement-bonded granular sample [Fig. 3(b)], we observe a similar general behavior during the first monotonic loading as above. However, significant intermittent fluctuations corresponding to stress drops are present, which make the identification of the previous plateau from C to D difficult, visible in Fig. 3(a) (see discussion below). These stress drops highlight transient stick-slip behavior, which may be caused by fracture nucleation or shear banding inside the loaded sample. Nevertheless, such stress drops are no longer observed during the subsequent unloading-reloading cycles (between E and F) in which a dry granular medium behavior is recovered, as for the ductile-cement-bonded sample.

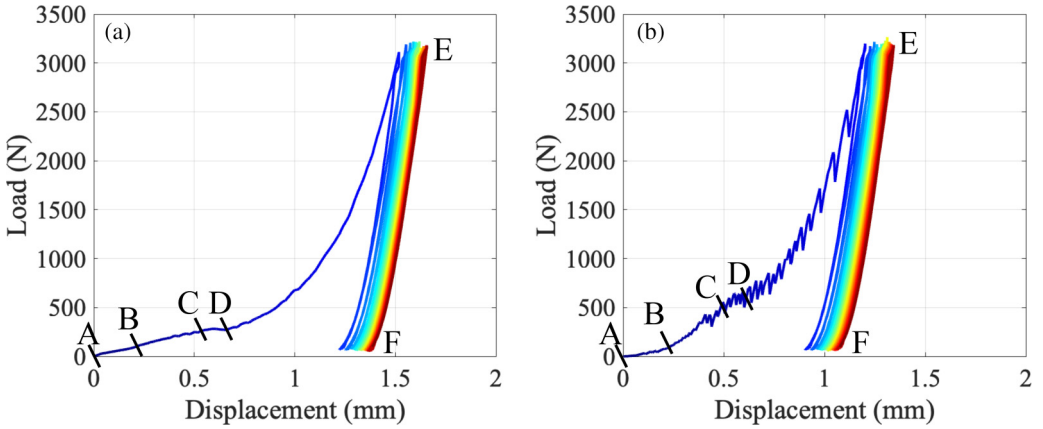

FIG. 3. Loads measured as functions of displacements (strain-driven) during the oedometric testing with (a) ductile-cement and (b) brittle-cement bonded granular samples, respectively. The response is remarkably different between the first loading (from A to E) and subsequent unloading-reloading (between E and F).

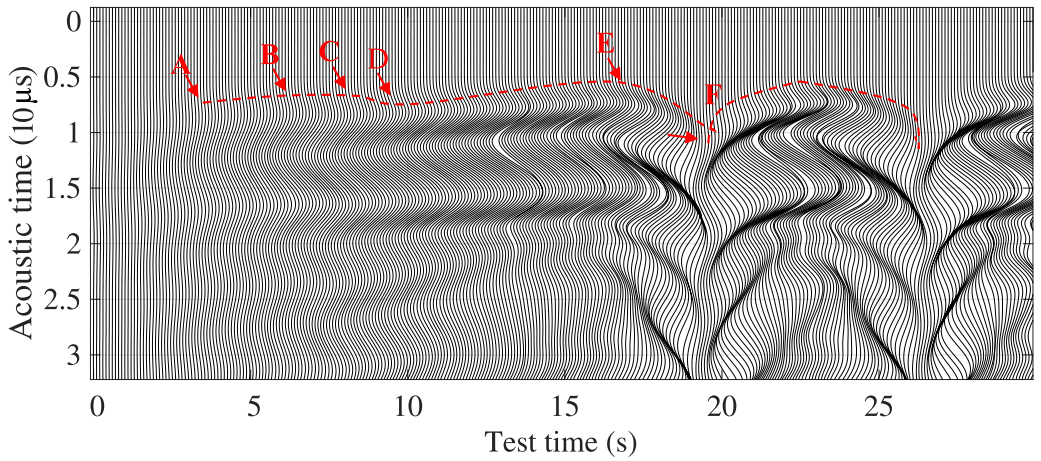

FIG. 4. Transmitted acoustic signals during the oedometric loading in a ductile-cement bonded sample. The red line indicates the arrivals of the direct P-waves (when 5% of the first peak amplitude is reached), and the letters refer to different loading steps indicated in Fig. 3(a).

2. *Ultrasound velocity measurement*

Our active acoustic probing relies on the investigation of one sinusoidal pulse propagation through the sample during the mechanical test. This small-amplitude wave is centered at $f = 100$ kHz with a corresponding wavelength about $\lambda \sim$ 10–20 mm for a compressional wave velocity measured as $V_P \sim 1000$ and 2000 m/s in dry noncohesive and cemented granular media, respectively [17,24]. In this frequency range, the wavelength is much larger than the bead size d ($\lambda \gg d$), and therefore, coherent waves are dominant compared with scattered waves. The detection of these coherent waves is also enhanced by the large transducer of diameter D ($\gg d$) [25]. Typical transmitted acoustic signals during the oedometric test in a ductile-cement-bonded sample are shown in Fig. 4. The test time ($\sim$30 s) refers to the mechanical loading where the indication A to F corresponds to different loading steps defined in the previous section, while the acoustic time refers to the wave propagation time ($\sim$30 μs). The wave propagation is much faster than the quasistatic mechanical loading and thus provides a snapshot of the sample elastic properties at different loading stages (mechanical relaxation of the sample is ignored here).

More specifically, we characterize the material state or properties such as damage via the compressional coherent wave (also called P waves) velocity V_P, measured by the time of flight of the signal picked at 5% of the first peak amplitude. The waveform is indeed not only shifted in time because of the velocity change but also deformed since its spectral content evolves with the state of the material due to the change in wave attenuation and scattering. This early time of flight is less influenced by the waveform distortion, allowing us to neglect such an effect as a first approximation.

The evolutions of the P-wave velocities are shown in Fig. 5 for the ductile- and brittle-cement-bonded granular samples. These velocities are greater than those in a noncohesive granular medium at the first loading for a comparable confining pressure [25] due to the bonds that enhance the P-wave velocity [17]. During the monotonic loading from A to E, the P-wave velocity in both cemented samples exhibits a complex evolution with the load or the controlled displacement. More precisely, V_P first increases (A–B), decreases slightly (B–C), then drastically (C–D), and eventually slightly increases (D–E). The following cycles (E–F) are described by the hysteretic loops accompanied with slight compaction, pointing to the behavior of a noncohesive frictional granular medium [25], where V_P scales on confining pressure as $V_P \sim P^{1/6}$. However, some significant differences on the evolution of V_P are observed between these two cemented samples. In the case of the brittle cement, V_P reaches a maximum value of $\sim$1550 m/s when loaded from A to B, which is higher than in the case of ductile cement $V_P \approx 1400$ m/s. This difference stems likely from the higher stiffness of the brittle cement (salol) which can also be seen from the mechanical responses during the first loading; for example, at the load of 500 N, the deformation is $\sim$2 times larger in Fig. 3(a) than that in Fig. 3(b). Nevertheless, V_P collapses abruptly to a low value of 1200 m/s (a decrease of 23%) when the confining pressure is beyond a critical value (around point C) due to the brittlelike breakage of bonds. Instead, V_P only decreases by 7% (down to 1300 m/s) under inelastic compaction in the ductile-cement-bonded sample, pointing to a partial damage or breakage of bonds. Moreover, we find that, for the brittle-cement-bonded sample, the fluctuation of the P-wave velocity is correlated to the intermittent stress drops, as shown in the inset of Fig. 5(b), where the decrease of V_P coincides almost with the stress drop. As mentioned above, the formation of shear bands is unlikely in the oedometric loading; thus, the intermittent stress drops accompanied by the simultaneous weakening of the P-wave velocity could be associated with the formation and evolution of compaction bands [13]. This is reminiscent of a brittlelike failure or stress drop observed during shear banding or localization [10], in which an avalanche or cascade of local ruptures occurs through the correlated elastic interaction, accompanied by AEs (see below).

3. *AE detection*

The passive probe consists of recording the AEs due to the irreversible events occurring inside the sample under external loading with an acoustic transducer [8,20,26]. They are equivalent to seismicity in the earth crust [27]. Monitoring

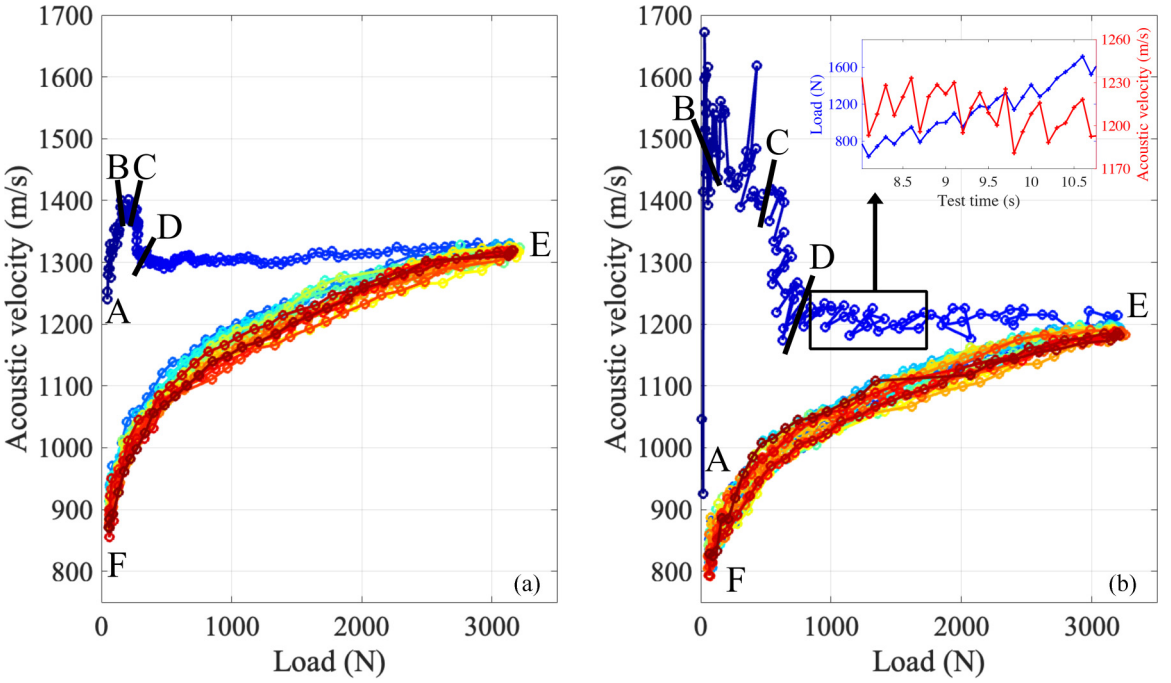

FIG. 5. The velocity of the compressional coherent wave measured as a function of the load (strain driven) in the (a) ductile-cement and (b) brittle-cement bonded samples. The first loading is in dark blue, the last cycle of unloading-loading is in red, other colors refer to the intermediary cycles. Inset in (b) shows the correlation between stress drops and P-wave velocity decreases.

the AE allows probing the precursor events such as crack nucleation on the microscopic (local) scale before the material failure, i.e., fractures on the macroscopic scale. However, unlike previous works (e.g., Ref. [13]), three-dimensional (3D) locations of AEs are not possible in this paper due to the multiple wave scattering associated with the strong heterogeneity in our cemented granular samples [17].

Figure 6 illustrates an example of AE recorded in a brittle-cement-bonded granular sample, loaded at a speed of 50 μm/s. The sampling frequencies for the mechanical and acoustic measurements are 2.5 Hz and 500 kHz, respectively. During the first monotonic loading, intermittent stress drop occurrence increases with increasing the load. They are correlated to the increasing AE activity likely due to the bond damage or/and rearrangement as observed in dry granular media [20] under oedometric compression. These characteristic stick-slip-like stress drops are, however, significantly reduced (or mostly disappear) in the subsequent cyclic unloading and reloading, and accordingly, the medium becomes almost aseismic (or silent). Nevertheless, there is a nonstationary background acoustic signal, identified as the press-induced noise increasing with the load. It has also been observed with the press in the absence of the granular sample but just loading the piezoelectric (ultrasonic) transducers. This instrumental noise is strewn with intermittent AE of various amplitudes and spectral contents. In the ductile-cement-bonded samples, AEs

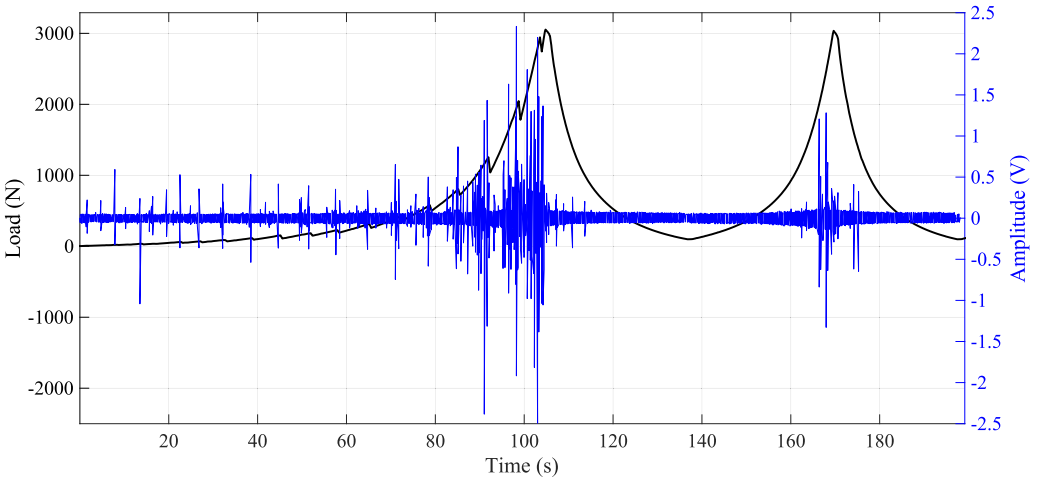

FIG. 6. Load (black) and acoustic emission (AE; blue) measured as a function of the time in a brittle-cement bonded granular sample during oedometric loading with a controlled axial displacement. Stick-slip-like stress drops are accompanied with significant AE.

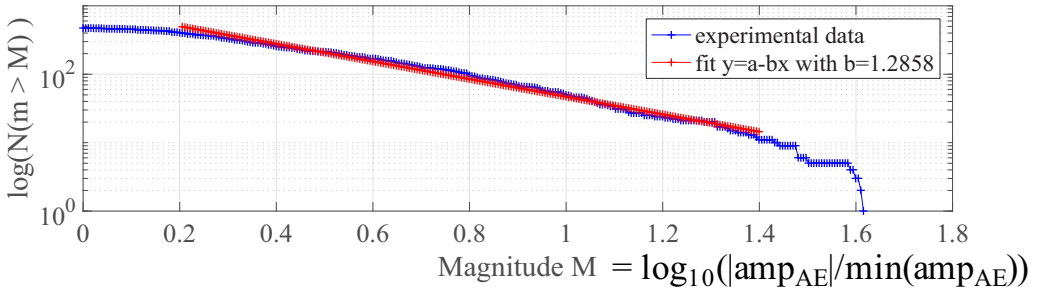

FIG. 7. Probability distribution of acoustic emission (AE) occurrence versus magnitude (in blue) plotted in a log-log scale with a characteristic contribution due to quasi-periodic stick-slip stress drops (indicated by the double arrow). Linear fit is based on the Gutenberg-Richter law (in red).

are also recorded even with much fewer events and without visible stress drops.

To detect and correctly analyze AE in the continuous set of data with an undesirable noise, several classical methods exist: with a simple amplitude threshold or with the ratio of a short-term average on a long-term average (STA/LTA). Among numerous methods proposed including machine learning, we choose to use a simple k-means clustering spectral method based on the spectrogram of the continuous signal [28,29].

We may characterize observed AE as *labquakes* and evaluate the maximum of the absolute amplitude A_{AE} of each AE. The relative magnitude of each event is calculated according to $M = \ln[A_{\mathrm{AE}}/\min(A_{\mathrm{AE}})]$. The probability distribution is plotted in Fig. 7, which may be compared with the Gutenberg-Richter law in seismology. It predicts that, for a sufficiently large number of events, $\ln[N(m > M)] = a - bM$, with $N(m > M)$ the number of events whose magnitude m is greater than M. Here, the b value is evaluated with a fit in the range of magnitude [0.2; 1.4] for which we assume there are enough detected AE events. Indeed, the number of detected AEs is underestimated both for lower magnitude due to the detection sensitivity and for large-magnitude events which are rare. For the earthquake statistics, the expected standard b value is 1. Our estimated value of $b \approx 1.3$ is consistent with other similar experimental studies [20,30]. The characteristic stick-slip events give rise to a hump tail (with a local maximum) at a relative magnitude of about $M = 1.6$.

C. Damage evolution under cyclic loading with increasing consolidation stress

1. Mechanical response

To better understand the damage process during inelastic compaction in cemented granular materials, we complete here the above experimental observations with increasing consolidation stress under cyclic loading. As shown in the insets of Fig. 8, we investigate the response of the sample to cumulative damages by increasing progressively the maximum force (i.e., consolidation stress) of cyclic loading, unloading and reloading, from $F = 500$ to 3000 N by a step of 500 N, while the minimal load is kept constant as in the above investigation. The sampling frequencies for mechanical measurements are 20 and 5 Hz for tests in ductile- and brittle-cement-bonded samples, respectively. For each loading cycle, the displacement varies linearly with time at a speed of 50 μm/s, which is ∼2 times slower than the loading rate in Fig. 3, except immediate inversions of the loading direction displacement due to the inertia of the electromechanical press that induces a short relaxation of ∼0.6 s.

Figure 8 depicts the cross-plots of loading force vs displacement in the case of the (a) ductile and (b) brittle cements. They highlight the anelastic and irreversible behavior under cyclic unloading and reloading, already observed in Fig. 3. The unloading curve presents systematically a different slope from the preceding loading path with increasingly steep slopes. If the load remains lower than the previous consolidation load, a slight hysteresis between unloading and reloading is observed at each cycle. Nevertheless, if the reloading exceeds the consolidation load (endpoint), they recover the masterlike curves which resemble the force-displacement responses under the monotonic loading in Fig. 3 (the vertical drop at the beginning of the unloading corresponds to the displacement inertia of the press and the induced relaxation). Note, however, these master curves obtained at a lower loading speed (i.e., 50 μm/s instead of 100 μm/s) show weakened rigidities compared with those observed in Fig. 3. This may be due to the viscoplastic behavior of cements (the lower the load speed, the higher the relaxation of deformation) and to the more pronounced damage associated with the ramped cyclic consolidation stress, particularly for the case of the brittle cement for which the compressive displacement is ∼3.7 mm in Fig. 8(b) but 1.2 mm in Fig. 3(b) when the load reaches $F =$ 3000 N. At the highest loading observed here, our cemented samples appear to be totally damaged, namely, nearly no more breakage of bonds are possible on further increasing the load. As a result, the master curves and the reloading paths merge with the same slope, corresponding to the usual behavior of a dry granular material under cyclic loading-unloading (i.e., states between E and F in Fig. 3).

Moreover, in the case of the brittle-cement-bonded sample [Fig. 8(b)], the stress drops (indicated by sawtoothlike stick-slip oscillations) are absent all along the unloading and during the reloading when the load is lower than the maximal load reached previously (also called consolidation stress). However, they reappear when unexplored greater values of the load are reached as if the sample has a memory of the loading history. This idea of memory and new states reached when

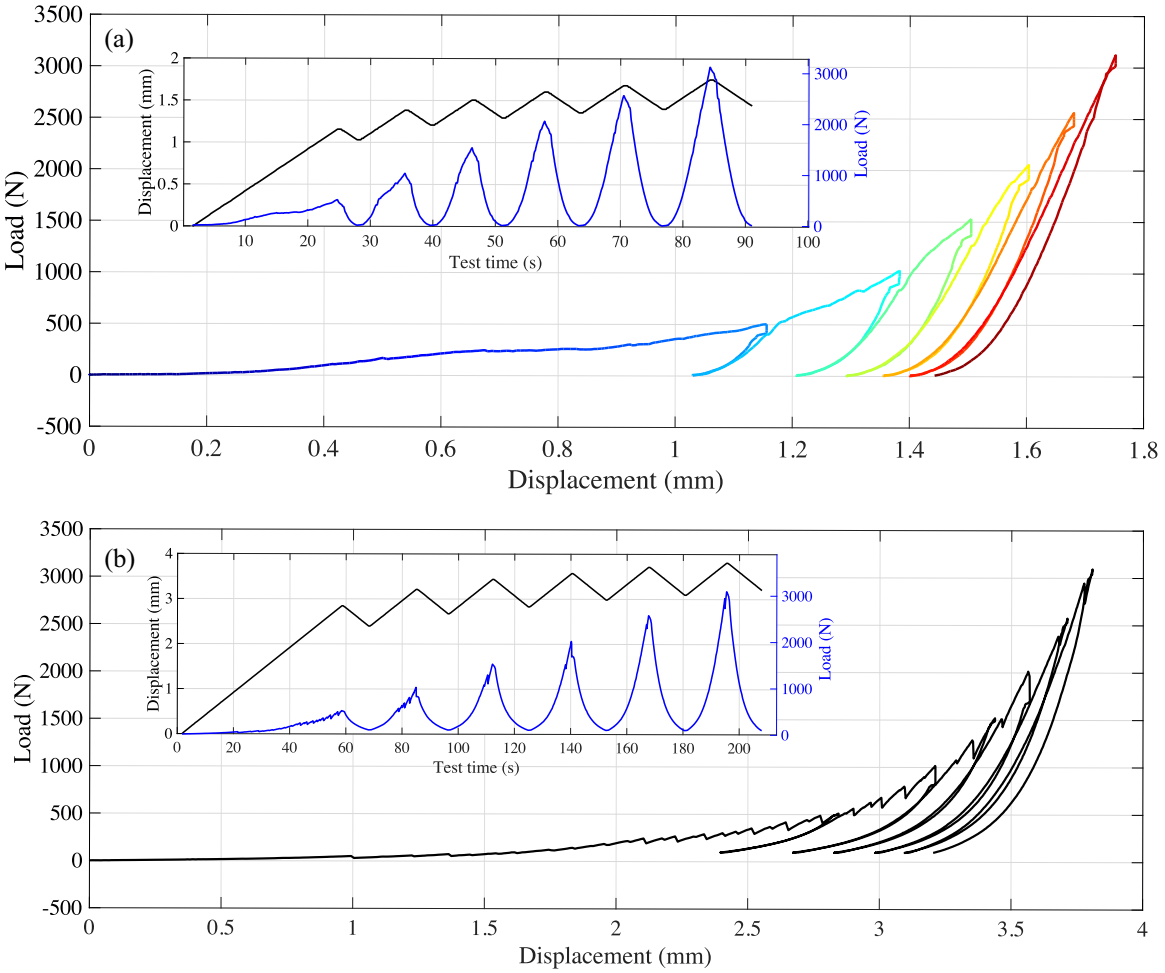

FIG. 8. Mechanical responses under oedometric cyclic loading with increasing consolidation stress of the (a) ductile-cement and (b) brittle-cement bonded granular samples. Insets show loading forces and displacements measured as functions of test time.

the load increases will be confirmed below by the AE analysis and Kaiser effect. The absence of apparent hysteretic loops suggests a negligible frictional dissipation here.

2. *Ultrasound velocity measurement*

As in Sec. II B, we can also investigate the material structural change during inelastic compaction loading by monitoring the evolution of the P-wave velocity. Figure 9 depicts the P-wave velocity measured as a function of the loading force (or axial stress) with increasing the consolidation stress in the ductile-cement-bonded granular samples. Compared with the data obtained with the constant consolidation stress protocol [Fig. 5(a)], we observe here an overall decrease of the P-wave velocity at a given load, with the increase of the consolidation stress of the cyclic loading. We note narrow hysteretic loops. Such hysteretic loops of P-wave velocity recover finally those obtained with constant consolidation stress at the same load range, as shown by the last cycle very similar to that in Fig. 5(a) (red curves). The main difference between the two loading protocols lies in the P-wave velocity V_{bond} (see Sec. III B), measured upon unloading at (almost) vanishing pressure $P \approx 75$ kPa ($F \approx 60$ N). Here, V_{bond} decreases progressively with repeated unloading-reloading cycles from $V_{\text{bond}} \approx 900$ to 750 m/s ($\Delta V_{\text{bond}}/V_{\text{bond}} \sim 17\%$), while it remains at relatively higher

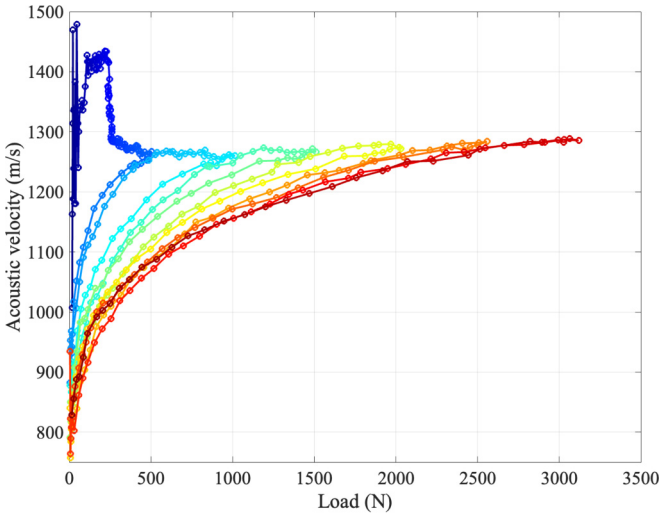

FIG. 9. P-wave velocity measured with the time of flight of the direct P-wave as a function of the loading force in a ductile-cement bonded sample.

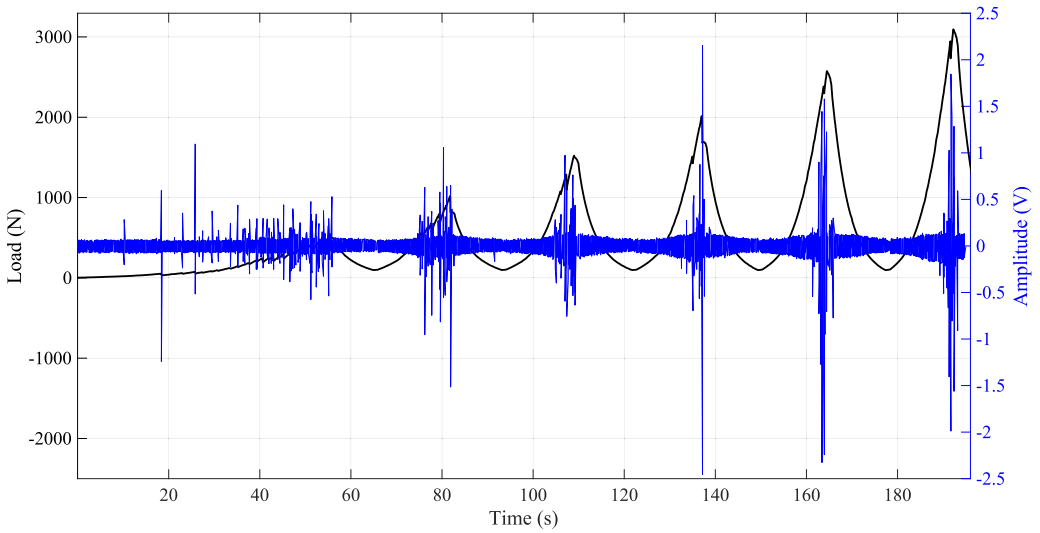

FIG. 10. Measured loading force (black) and acoustic emission (AE; blue) as functions of test time in a brittle-cement bonded sample, under cyclic loading with increasing consolidation stress.

value and varies little from 940 to 860 m/s ($\Delta V_{\text{bond}}/V_{\text{bond}} \sim 8.5\%$) in Fig. 5(a). This observation suggests that oscillatory (cyclic) loading may facilitate the damage process via the progressive bond breakage (see discussion below), reminiscent of a fatigue process.

3. AE detection

As a passive acoustic probing, we also show in Fig. 10 the AE recorded in the brittle-cement-bonded sample under increasing consolidation stress. It is sampled at 200 kHz continuously all along the mechanical test lasting for ∼3 min. The noise of the electromechanical press is clearly visible as its amplitude evolves with the imposed load, as in the cyclic loading test with a constant consolidation stress. As seismicity, these AE are strongly correlated to the intermittent stress drops [Fig. 10(a)]. We will analyze these AEs in more detail below (Sec. III C), particularly with the memory effect observed above in Sec. II C.

III. DISCUSSION AND MODELING

Inelastic compactions have been observed under oedometric loading beyond a certain threshold, both monotonic (Fig. 3) and cyclic with increasing consolidation stress (Fig. 8), in cemented granular materials. The induced damage and plastic deformation investigated here are associated with both the breakage of cement (ductile and brittle) bonding and the rearrangement of grains, without the grain crushing. Opposite, it has been shown that inelastic compaction in porous sandstone during triaxial experiments or hydrostatic compaction (zero deviatoric stress) is associated with grain crushing and pore collapse [14,15,31]. They observed two possible failure modes: localized compaction bands at low confinement and more complex diffuse compactions at higher confinement, accompanied by abundant AE events.

Our experimental observation of simultaneous intermittent stress drops, the P-wave velocity decreases, and AE detection in the brittle-cement-bonded sample indicate that the inelastic compaction observed here is dominated by the material bulk structural change and damage, not by the sliding (stick-slip) of the sample at the interface with the oedometer cell. To monitor such material damage, both active and passive acoustic detections indeed provide adequate and unique probing.

A. Interplay between bond damage and contact hardening under compression

Physically, two distinct and competitive mechanisms affect the elastic wave velocities during inelastic compaction: debonding (cracking) and Hertzian contact (porosity decrease). We seek to interpret the evolution of P-wave velocity observed (Fig. 5) within the effective medium framework where small amounts of cement are assumed to be distributed homogeneously between grain contacts, forming independent bonds in the (so-called) pendular regime [Fig. 11(a)] [18].

On the scale of cemented grain contact [Fig. 11(b)], we consider a heuristic model proposed by Dvorkin *et al.* [32,33] with parallel association of two mechanical elements: the first is a nonlinear spring k_{H} for describing the Hertzian-like contact between beads, and the second corresponds to an elastoplastic element k_{B} for modeling the cemented bond. The contact stiffness $k_{\text{H}}(P)$ increases with increasing the (isotropic) compression P, while k_{B} is a constant (linear spring) that breaks down irreversibly to zero (the healing effect is not considered here) beyond the yield threshold. Therefore, the stiffness of a cemented contact resulting from the combination of these two parallel elements $k_{\text{C}} \sim k_{\text{H}} + k_{\text{B}}$ may increase with increasing the compression P, then saturate or decrease due to the evolutions of k_{H} and k_{B} in counteracting dependence with P.

Within the effective medium theory (EMT), the compression and shear wave velocities are $V_P = [(K + 4G/3)/\rho]^{1/2}$ and $V_S = (G/\rho)^{1/2}$, where the bulk (K) and shear (G) effective modulus are linearly proportional to the microscopic contact stiffness $k_{\text{C}}(P)$ via the coordination number Z and, implicitly, the porosity $(1 - \phi_s)$ [see Eq. (2) below]. Consequently, the evolution of the P-wave velocity in Fig. 5 may be correlated to the change of the contact stiffness $k_{\text{C}}(P)$ and interpreted as

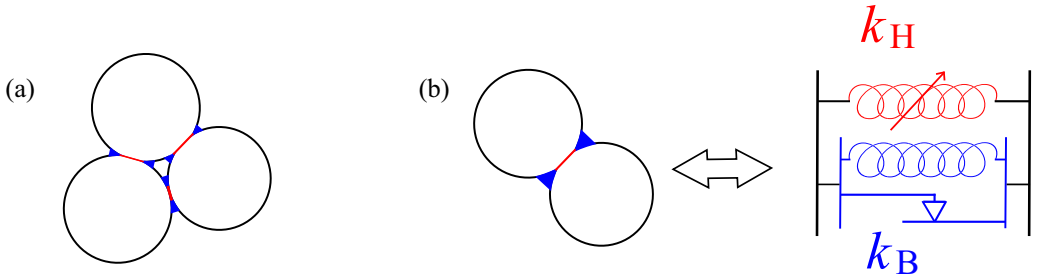

FIG. 11. Schematic illustrations of cemented granular materials: (a) cement bonds are independent (not link between them), i.e., in the pendular regime; (b) cemented contact is modeled as a parallel association of a hertzian contact and an elastoplastic element.

follows. At first, increasing the oedometric loading P makes V_P increase due to the increase of k_H and the possible creation of new contacts affecting the coordination number Z [34], where the cemented bonds behave elastically [17,33] with constant k_B (from A to B). When the damage process (debonding or crack nucleation) becomes dominant, V_P first decreases slightly (from B to C) and then drastically with the likely formation of compaction bands, i.e., macrofractures within a set of intact beads (plateau from C to D), as those occurred in porous sandstone with pore collapse (and grain crushing). Further increasing the load, V_P asymptotically reaches a noncohesive granular state [22] where most of cemented bonds are broken or nearly damaged, as can be expected.

Indeed, upon unloading and reloading (between E and F), we recover a similar evolution of P-wave velocity V_P vs the confining stress P, as those observed in noncohesive (dry) granular materials $V_P \sim P^\beta$, with β between $\frac{1}{4}$ and $\frac{1}{6}$ [25,34,35]. Note, however, there still exists residual bonding [17] since the P-wave velocity V_{bond} remains important (Fig. 5) upon unloading at $P \approx 0$ (see Sec. III B). The above situation is different from those observed in Fig. 9. When unloading-reloading is performed at low consolidation stress (i.e., blue curves), for which a large number of cemented bonds is not yet damaged, V_P does not reach the noncohesive granular states obtained between E and F (red curves) in Fig. 5(a). Instead, V_P at the endpoints (i.e., when the unloading-reloading is finished and the reloading reaches the previously applied consolidation stress) follows the path D–E (blue curve). This observation shows that the partially damaged sample has a memory of its prestressed state.

B. Evolution of residual cohesive bonding under cyclic loading: Digby's model

As mentioned above, to investigate the damage or debonding degree by the oedometric loading, we may evaluate the P-wave velocity V_{bond} at $P \sim 0$. To support this idea, we consider the bonded contact model proposed by Digby [36]. As illustrated in Fig. 12, the contact area between two elastic spheres (of radius a) includes a bonded portion (of radius b) to simulate a cementing or sintering effect between grains [37]. When increasing the pressure (which is approximated as the axial stress P), the total area of contact increases to radius a ($\geqslant b$). The radius b is independent of the applied compression; $b = 0$ corresponds to the case of noncohesive particles. By analogy with the Hertz theory and the Mindlin model, the normal and tangential contact stiffnesses k_n and k_t, respectively, are given by

$$k_n = 4\mu a/(1-\nu), \tag{1a}$$

$$k_t = 8\mu b/(2-\nu), \tag{1b}$$

if the annular contact region between radii a and b is assumed to be perfectly sliding. Here, ν and μ are the Poisson ratio and the shear modulus of the grain material. By statistical analysis (i.e., effective medium approach), the effective bulk K and shear modulus G can be derived from the contact stiffnesses k_n and k_t as $K = Z\phi_s k_n/(12\pi R)$ and $G = Z\phi_s(k_n + 3k_t/2)/(20\pi R)$, with R the bead radius [38]. From Eqs. (1a) and (1b), the elastic moduli K and G and, accordingly, the elastic wave velocities V_P and V_S may also be given by the contact radii a and b [36]:

$$V_P^2 = \left(\frac{\mu Z}{5\pi R\varrho_g}\right)\left[\frac{3a}{1-\nu} + \frac{4b}{2-\nu}\right], \tag{2a}$$

$$V_S^2 = \left(\frac{\mu Z}{5\pi R\varrho_g}\right)\left[\frac{a}{1-\nu} + \frac{3b}{2-\nu}\right], \tag{2b}$$

where a depends on the applied pressure as $\sim P^{1/3}$ (Hertzian contact) and b is attributed to the bonded contact area. Together with the coordination number Z and the bead property, this bonding (cohesion) parameter b gives a wave velocity $V_{\text{bond}} \sim (Zb)^{1/2}$ at vanishing pressure, providing thus a measurable indicator of debonding (damage) by acoustic velocity, as mentioned above.

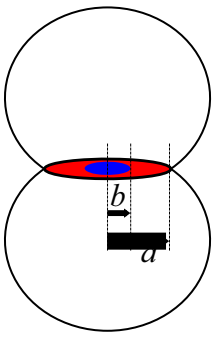

FIG. 12. Digby's bonded contact model with a total circular contact area of radius a made of an annular sliding area (in red) and a bonded area (in blue) of radius b.

The analytical damage model of cemented granular materials (on the macroscopic scale) is not available despite several theoretical efforts (e.g., Ref. [32]) and numerical simulations [11,12,21,39]. The simulation of oedometric compression experiments developed by Canel *et al.* [39] points out that the strain fields are very heterogeneous and that a small amount of damage of bonds on the local scale induces a dramatic decrease in the coherent wave velocity on the global scale, which provides thus a very sensitive probe to monitor the damage processes in such heterogeneous materials.

Nevertheless, the above EMT based on Digby's bonded contact model was used to empirically interpret the evolution of elastic wave velocities measured in porous sandstone during inelastic compaction [31]. More specifically, the significant increase of the V_P/V_S ratio [which depends on the quantity a/b according to Eq. (2)] beyond a certain threshold stress can be related to the decrease of b, i.e., the bonding radius. This implies that the grains became less and less cemented with increasing the external loading, which was consistent with their observed grain crushing.

To investigate furthermore the debonding (damage) in this paper, we identify as a first approximation k_{H} and the elasto-plastic element k_{B} in Fig. 11(b) as k_n and k_t in Eqs. (1a) and (1b), respectively. To fit the measured P-wave velocities in cemented samples (Fig. 5), we rewrite the P-wave velocity as

$$V_P^2 = \alpha F^{2\beta} + V_{\mathrm{bond}}^2. \tag{3}$$

Here, the first term originates from the Hertz contact law with F the axial loading force and α a constant, whereas the second term refers to the cemented bond-induced velocity V_{bond} (found at vanishing pressure), characterizing the degree of bond damage under loading, monitored at vanishing load (unloading) $F = 0$. Unlike previous works in porous sandstone, the damage process would be here dominated by the debonding of cements between grain contacts rather than grain crushing [13]. This should make the above Digby's model more relevant for the case considered in this paper.

There are two main parameters V_{bond} and β to infer in Eq. (3) from P-wave velocities measured in the weakly cemented granular state, between E and F (Fig. 5). More specifically, we fit with the data obtained during unloading to monitor the damage degree by the previous loading. By choosing an exponent $\beta = \frac{1}{6}$, we can deduce V_{bond} as the only free parameter of a curve-fitting procedure, with α found nearly constant for each unloading cycle. Figure 13 shows V_{bond} inferred from tens of cycles in the ductile-cement-bonded sample with constant and increasing consolidation stresses, respectively. With constant consolidation stresses [Fig. 5(a)], the fitted V_{bond} varies slightly with loading-unloading cycles around a value of 600 m/s, corresponding to $F = 0$ in Eq. (3) (except the discrepancy at cycle #6, likely due to a manipulation defect). They are lower than the previously estimated $V_{\mathrm{bond}d}$ measured at the vanishing load $F \sim 60$ N. One should note that this fit procedure assumes V_{bond} to be constant during a given unloading; however, it may vary with new damages, for instance.

We now examine the P-wave velocity evolution, still with the model of Eq. (3), under cyclic unloading-reloading with increasing consolidation stress and focus on the ductile-cement-bonded sample (Fig. 9). Using the same fitting procedure described above, we infer the cohesion velocity V_{bond}. After the first unloading with V_{bond} found close to 900 m/s, Fig. 13 illustrates a considerable decrease of V_{bond} with successive loading cycles, from 860 to 560 m/s. This acoustic probing confirms that additional damage (debonding) is created with increasing the consolidation stress, as can be expected. Interestingly, it also reveals that, for a given consolidation stress, the cyclic ramping protocol is more efficient than the monotonic loading to transition the cemented materials to noncohesive granular packings. The structural relaxation upon unloading may facilitate the diffusion of cracks (debonding), e.g., via rearrangement of grains [23], which enhances the fracture nucleation upon reloading, reminiscent of a fatiguelike process.

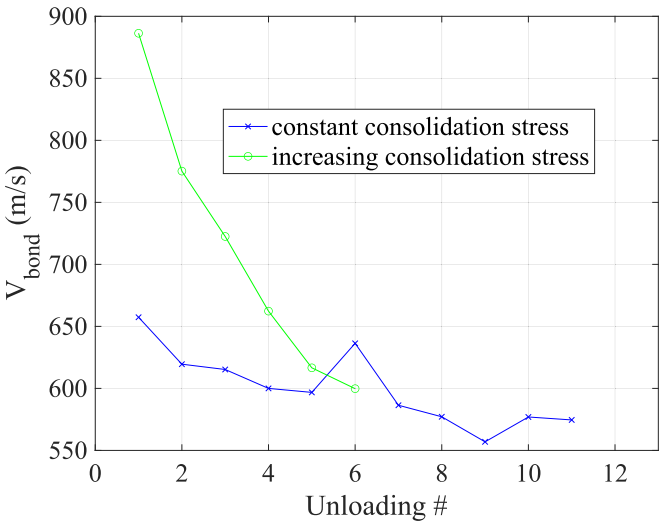

FIG. 13. V_{bond} measured as a function of loading cycles in the ductile-cement bonded sample, under cyclic loading with constant (blue crosses) and increasing (green dots) consolidation stresses, inferred from measured data $V_P(F)$ via Eq. (3) with $\beta = \frac{1}{6}$.

C. AEs during inelastic compaction: Omori-like law and Kaiser effect

In this paper, the discontinuous, burstlike AE events (i.e., seismicity) have been observed in brittle-cement-bonded granular samples, which are strongly correlated with recorded stick-slip-like stress drops. Investigation of the cumulated number of such AEs and the rates (number of AEs per second) is of considerable importance for understanding precursor events. Figure 14(a) illustrates the accumulated number of events measured under cyclic loading with constant consolidation stress (Fig. 6). It increases drastically during the stick phase up to a large stress drop, i.e., the *mainshock*. The rate of these AE (precursors) is influenced by both the loading stress P or force F and the proximity F-F_{drop} to the stress drop (failure) characterized by the sudden decrease ΔF_{drop}.

Here, we focus on the evolution of the (normalized) AE rate during the stick phase for the 10 stick-slip events, from #5 to #14 [Fig. 14(b)]. The events from #1 to #4 are not considered because the stress drops and, consequently, AEs are too weak to be detected efficiently through the k-means clustering method. The last event #15 is also neglected here due to the

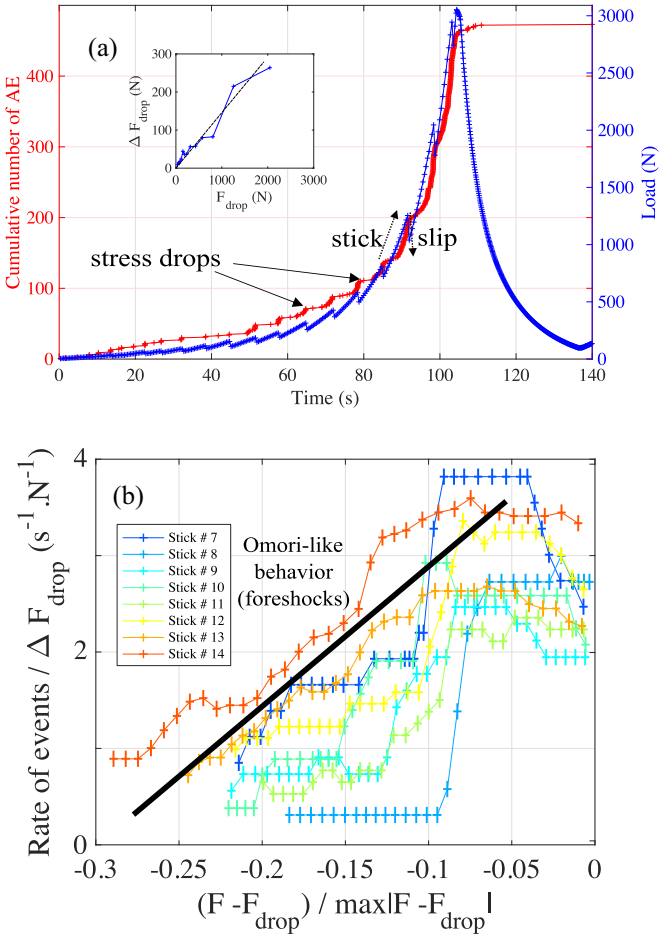

FIG. 14. (a) Load (in blue) and cumulated number of acoustic emissions (in red) as functions of the time in a brittle-cement bonded sample. Inset: The magnitude of stress drops as a function of the threshold stress (failure). The dashed line indicates an effective friction law with a friction coefficient $\mu \approx 0.15$. (b) Temporal events rates during the stick phases #7 to 14 normalized by the corresponding stress drop magnitude as functions of the normalized distance of load to failure, i.e., large stress drop (see text). The black curve suggests an Omori-like law for foreshocks.

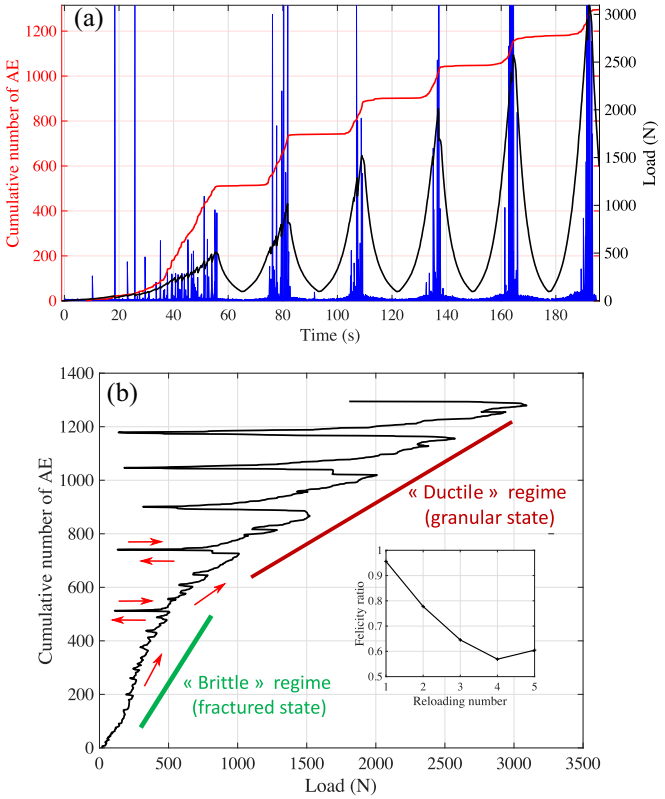

FIG. 15. (a) Load (black curve), absolute value of the acoustic emission (AE) recording (blue curve) and cumulative number of AE (red curve) as functions of the time. (b) Cumulative number of AE as a function of the load. Red arrows indicate the followed path in time until the second reloading. The inset shows the five Felicity ratios available from this test.

measurement incertitude affected by the sampling frequency of our electromechanical press (2.5 Hz) which is likely too low to correctly measure the loading stress change during this abrupt stress drop event. These AE rates are calculated over a moving window of 3 s with an overlapping of 97%, which makes it continuously decrease at the end of each stick phase by averaging effect with the rates of the following consecutive phase.

Remember that the magnitude of shear stress drops $\Delta\tau$ associated with the stick-slip instability in sheared granular layers remains comparable at the constant normal stress P [2]. Interestingly, we observe here an almost linear increase of the stress (force) drop ΔF_{drop} with increasing axial load F during inelastic compaction, shown in the inset of Fig. 14(a). This indeed formally reminds us of a form of friction process. If we assume $\Delta\tau \sim (\mu_s - \mu_d)\, P$ (with μ_s and μ_d the Coulomb-like static and dynamic friction coefficients), by analogy, $\Delta\tau$ vs ΔF_{drop} and P vs F, we may speculate an increase of ΔF_{drop} with increasing F assuming a friction coefficient ~0.15. Based on this analogy, we plot the normalized AE rates by ΔF_{drop} as a function of the distance to the stress drop $(F - F_{\text{drop}})$ normalized by max $(|F - F_{\text{drop}}|)$ for the series of stress drops. Figure 14(b) shows such plots where all AE data seem to gather around a unique (master) curve, suggesting thus a scaling law which may be reminiscent of an Omori-like law for foreshocks [20]. Considering the difference of loading protocols between direct-shear and oedometric testing, further investigation is needed to better understand the quasiregular stick-slip behavior likely associated with inelastic compaction bands.

Figure 15(a) shows the AE recorded during cyclic loading with increasing consolidation stress (as in Fig. 8) and the cumulative number detected with a STA/LTA process: 0.1 ms for the STA, 5 ms for the LTA and a detection threshold of 0.1 [28]. The cumulative number of 1295 AEs recorded as a function of the loading history [Fig. 15(b)], i.e., loading, unloading, and reloading, confirm more precisely the material memory property seen in mechanical (Fig. 8) and P-wave velocity measurements (Fig. 9) for the two first cyclic loadings where the AE rates recover the master curve at endpoints upon reloading. Such observations, known as the Kaiser effect, exist widely in amorphous solids such as metal alloys [40] and rocks [41–43]. AEs are generally linked to the creation

and development of fractures in a solidlike material under loading. It has been shown by the localization of AE sources that, during unloading, there are nearly no AEs due to the absence of the crack growth, but during reloading, AEs occur in the previously damaged zones with the growth of fractures, particularly when the load becomes greater than the previous consolidation stress [44].

However, we here observe that the Kaiser effect is less and less respected when the load is beyond a certain threshold ($F \sim 900$ N), meaning that the sample is so damaged that it starts losing its memory property. The cemented granular material undergoes thus a transition from cohesive (solidlike) to granularlike (fluidlike) states where the stress principal axes may evolve with the loading history [45–47]. Such an evolution is also indicated by the decrease of P-wave velocity V_{bond} at vanishing pressure [Fig. 13(b)].

To characterize the occurrence of AEs upon reloading at a lower load (already explored) than the previous consolidation stress (maximal), we may evaluate the Felicity ratio which is considered a measure of the (rock) material quality [42]. It is defined as the ratio between the applied load at which new AEs occur during reloading and the previous maximum applied load (consolidation stress). In this paper, we consider arbitrarily that new AE appearance becomes significant from 10 more AEs upon reloading for calculating the Felicity ratio. This ratio is equal to 1 for the perfect Kaiser effect (in practice, we consider that ratio for a value >0.9). The five Felicity ratios available from this test are plotted in the inset of Fig. 15(b). The first cycle highlights a nearly perfect Kaiser effect, i.e., the memory effect, as observed above in mechanical (Fig. 8) and acoustic P-wave velocity measurements (Fig. 9), with the Felicity ratio equal to 0.96. It then decreases down to 0.57 at the fourth reloading before increasing slightly to 0.61 at the last reloading.

Finally, we remind readers that the Kaiser and Felicity ratios are usually investigated with triaxial tests and not with oedometric loading. The main difference is that, in triaxial tests, compression strength is well defined, corresponding to the maximal load reached before the load decrease, whereas in oedometric tests, such a compression strength is not clearly observed. Nevertheless, our results suggest that the Kaiser and Felicity effects observed here could correspond to the compaction banding, localized or diffuse, like those in porous sandstone [14,15,31] but without grain crushing observed in our works. Such evaluations also provide a possible measure of the material damage, i.e., the distance to failure. However, it is still not clear why no significant AEs are detected in our ductile-cement-bonded samples (aseismic) during inelastic compaction.

IV. CONCLUSIONS

In summary, we have investigated the inelastic compaction of cemented granular materials under the oedometric loading, monitored simultaneously by measuring the P-wave velocity (active detection) and recording AE, if any (passive detection). The nonlinear mechanical behavior with an increasing loading is related to the transition from a cohesive to a partially noncohesive granular material via the debonding of cemented grain contacts. This damage process is manifested clearly by the elastic weakening on the macroscopic scale through the decrease of the P-wave velocity. Using Digby's cemented granular model, we can correctly explain our P-wave velocity measurements and make the cohesion velocity V_{bond}, measured at vanishing pressure, as an indicator of the debonding on the scale of grain contact. A main finding is that, as a function of the bond material, ductile or brittle, a cemented granular sample behaves fundamentally differently. In the former, the transition during inelastic compaction undergoes continuously, suggesting diffuse compaction bands, while in the latter, the cohesive-to-noncohesive state transition via plastic deformation is accompanied by intermittent stress drops (stick-slip) pointing to the localized compactive shear bands on the mesoscopic scale. These observations may be understood by a short-range interaction for the ductile-cement bonds (due to viscous damping) but a long-range interaction for the brittle-cement bonds (via elastic response).

The fundamental difference between these two types of cemented granular samples is also revealed by their activity of AE: the former is nearly aseismic, while the latter has microseismic activity. AEs characterize the damage process and microscopic physics on the grain contact scale. The aseismicity in ductile-cement-bonded samples may be explained by two effects: The first is the overdamped motion of grains after the bond breakage (AE source) due to the viscous ductile cement, and the second is the high attenuation of emitted wave propagation (if any) through the contact network caused by these dissipative bonds [48]. Instead, AEs observed in brittle-cement-bonded samples clearly demonstrate their correlation with the stick-slip-like stress drops, as observed in sheared granular layers and seismic faults. These AEs show a statistical distribution in agreement with the Gutenberg-Richter law, demonstrating thus the powerful similarity between these labquakes and seismicity [27]. They also indicate a drastic increase of AE rates when the load approaches a failure, i.e., a large stress-drop event or mainshock, the temporal distribution being close to the linear Omori-like law for foreshocks. With the consolidation stress ramped up during the cyclic loading, AE rates slow down together with the loss of the (Kaiser) memory effect. This occurs precisely at the transition of a cemented porous material to a noncohesive granular medium through fracture nucleation process [22].

Surprisingly, quasiperiodic large stress drops akin to stick-slip events in granular faults under shear have been observed here during oedometric loading. Contrary to what happens in noncohesive granular materials, these stick-slip instabilities may be associated with the formation of compaction bands due to the cohesion-induced long-range interaction, resulting in a brittlelike fracture nucleation [13,15]. Further investigation is needed to better understand the underlying physics in the presence of shear banding, which is also of interest for earthquake rupture [49]. Active monitoring by multiple scattered ultrasounds and Discret Element Method simulations on the grain-contact scale [25,50] may help for such a study.

ACKNOWLEDGMENTS

The authors acknowledge support from the European Research Council under the European Union Horizon 2020

research and innovation program (Grant Agreement No. 742335, F-IMAGE) and from PSL University under the program "Investissements d'Avenir" launched by the French Government.

[1] Y. Ben-Zion, Collective behavior of earthquakes and faults: Continuum-discrete transitions, progressive evolutionary changes, and different dynamic regimes, Rev. Geophys. **46**, RG4006 (2008).

[2] C. Marone, Laboratory-derived friction laws and their applications to seismic faulting, Annu. Rev. Earth Planet. Sci. **26**, 643 (1998).

[3] T. M. Mitchell and D. R. Faulkner, The nature and origin of off-fault damage surrounding strike-slip fault zones with a wide range of displacements: A field study from the Atacama fault zone, northern Chile, J. Struct. Geol. **31**, 802 (2009).

[4] M. Thomas, H. Bhat, and Y. Klinger, Effect of brittle off-fault damage on earthquake rupture dynamics, in *Fault Zone Dynamic Processes*, edited by M. Y. Thomas, T. M. Mitchell, and H. S. Bhat (American Geophysical Union, Washington DC, 2017), Chap. 14, pp. 255–280.

[5] W. F. Brace and J. D. Byerlee, Stick-slip as a mechanism for earthquakes, Science **153**, 990 (1966).

[6] J. Dieterich, Modeling of rock friction 1. Experimental results and constitutive equations, J. Geophys. Res. **84**, 2161 (1979).

[7] A. Ruina, Slip instability and state variable friction laws, J. Geophys. Res. **88**, 10359 (1983).

[8] D. Lockner, The role of acoustic emission in the study of rock fracture, Int. J. Rock Mech. Min. Sci. Geomech. Abstr. **30**, 883 (1993).

[9] I. Main, Statistical physics, seismogenesis, and seismic hazard, Rev. Geophys. **34**, 433 (1996).

[10] D. Amitrano, J.-R. Grasso, and D. Hantz, From diffuse to localized damage through elastic interaction, Geophys. Res. Lett. **26**, 2109 (1999).

[11] F. Kun, I. Varga, S. Lennartz-Sassinek, and I. Main, Approaches failure in porous granular materials under compression, Phys. Rev. E **88**, 062207 (2013).

[12] Y. Yamaguchi, S. Biswas, T. Hatano, and L. Goehring, Failure proceses of cemented granular materials, Phys. Rev. E **102**, 052903 (2020).

[13] J. Fortin, S. Stanchits, G. Dressen, and Y. Guéguen, Acoustic emission and velocities associated with the formation of compaction bands in sandstone, J. Geophys. Res. **111**, B10203 (2006).

[14] M. Adelinet, J. Fortin, A. Schubnel, and Y. Guéguen, Deformation modes in an Icelandic basalt: From brittle failure to localized deformation bands, J. Volcan. Geotherm. Res. **255**, 15 (2013).

[15] P. Baud, A. Schubnel, M. Heap, and A. Rolland, Inelastic compaction in high-porosity limestone monitored using acoustic emissions, J. Geophys. Res.: Solid Erath **122**, 9989 (2017).

[16] K. A. Issen and J. W. Rudnicki, Conditions for compaction bands in porous rock, J. Geophys. Res. **105**, 21529 (2000).

[17] V. Langlois and X. Jia, Acoustic probing of elastic behavior and damage in weakly cemented granular media, Phys. Rev. E **89**, 023206 (2014).

[18] A. Hemmerle, M. Schröter, and L. Goehring, A cohesive granular material with tunable elasticity, Sci. Rep. **6**, 35650 (2016).

[19] Y. Khidas and X. Jia, Probing the shear-band formation in granular media with sound waves, Phys. Rev. E **85**, 051302 (2012).

[20] P. A. Johnson, B. Ferdowsi, B. M. Kaproth, M. Scuderi, M. Griffa, J. Carmeliet, R. A. Guyer, P.-Y. Le Bas, D. T. Trugman, C. Marone, Acoustic emission and microslip precursors to stick-slip failure in sheared granular media, Geophys. Res. Lett. **40**, 5627 (2013).

[21] V. Topin, J. Y. Delenne, F. Radjai, L. Brendel, and F. Mabille, Strength and failure of cemented granular matter, Euro Phys. J. E **23**, 413 (2007).

[22] V. Lyakhovsky and Y. Ben-Zion, A continuum damage-breakage faulting model and solid-granular transitions, Pure Appl. Geophys. **171**, 3099 (2014).

[23] E. R. Nowak, J. B. Knight, E. Ben-Naim, H. M. Jaeger, and S. R. Nagel, Density fluctuations in vibrated granular materials, Phys. Rev. E **57**, 1971 (1998).

[24] A. Miksic, Étude des propriétés mécaniques et acoustiques d'un milieu granulaire sous chargements cycliques, Ph.D. thesis, Université Paris-Est Marne-la-Vallée, France, 2008.

[25] X. Jia, C. Caroli, and B. Velocky, Ultrasound propagation in externally stressed granular media, Phys. Rev. Lett. **82**, 1863 (1999).

[26] G. Michlmayr, D. Cohen, and D. Or, Sources and characteristics of acoustic emissions from mechanically stressed geologic granular media—A review, Earth-Sci. Rev. **112**, 97 (2012).

[27] E. Vives, J. Baró, and A. Planes, From labquakes in porous materials to earthquakes, in *Avalanches in Functional Materials and Geophysics*, edited by E. K. H. Salje, A. Saxena, and A. Planes (Springer International Publishing, Cham, 2018), Chap. 3, pp. 31–58.

[28] V. Canel, *Acoustic Monitoring of Damage in Cemented Granular Materials: Experiments and Simulations*, Ph.D. thesis, Université Grenoble Alpes, France, 2020.

[29] P.-N. Tan, M. Steinbach, A. Karpatne, and V. Kumar, *Introduction to Data Mining*, 2nd ed. (Pearson, New York, 2019).

[30] J. Rivière, Z. Lv, P. Johnson, and C. Marone, Evolution of *b*-value during the seismic cycle: Insights from laboratory experiments on simulated faults, Earth Planet. Sci. Lett. **482**, 407 (2018).

[31] J. Fortin, Y. Guéguen, and A. Shubnel, Effects of pore collapse and grain crushing on ultrasonic velocities and V_P/V_S, J. Geophys. Res. **112**, B08207 (2007).

[32] D. Dvorkin, G. Mavko, and G. A. Nur, The effect of cementation on the elastic properties of granular material, Mech. Mater. **12**, 207 (1991).

[33] D. Dvorkin and D. Yale, Plastic compaction of cemented granular materials, Comput. Geotech. **20**, 287 (1997).

[34] J. D. Goddard, Nonlinear elasticity and pressure-dependent wave speeds in granular media, Proc. R. Soc. Lond. A **430**, 105 (1990).

[35] H. Makse, N. Gland, D. L. Johnson, and L. Schwartz, Granular packings: Nonlinear elasticity, sound propagation, and collective relaxation dynamics, Phys. Rev. E **70**, 061302 (2004).

[36] P. Digby, The effective elastic moduli of porous granular rocks, J. Appl. Mech. **48**, 803 (1981).

[37] V. Langlois and X. Jia, Ultrasonic monitoring of the elastic properties of PMMA bead packings and their rearrangement during pressure sintering, Powder Technol. **208**, 509 (2011).

[38] K. W. Winkler, Contact stiffness in granular porous materials: Comparison between theory and experiment, Geophys. Res. Lett. **10**, 1073 (1983).

[39] V. Canel, M. Campillo, X. Jia, and I. Ionescu, Damage in cohesive granular materials: Simulations and geophysical implications, C.R. Geosci. **356**, 1 (2023).

[40] J. Kaiser, Information and conclusions from the measurement of noises in tensile stressing of metallic materials, Arch Eisenhuttenwesen **24**, 43 (1953).

[41] K. Kurita and N. Fujii, Stress memory of crystalline rocks in acoustic emission, Geophys. Res. Lett. **6**, 9 (1979).

[42] C. Li and E. Nordlund, Experimental verification of the Kaiser effect in rocks, Rock Mech. Eng. **26**, 333 (1993).

[43] A. Lavrov, The Kaiser effect in rocks: Principles and stress estimation techniques, Int. J. Rock Mech. Mining Sci. **40**, 151 (2003).

[44] M. Seto, M. Utagawa, and K. Katsuyama, The relation between the variation of AE hypocenters and the Kaiser effect of Shirahama sandstone, in *8th ISRM Congress. International Society for Rock Mechanics and Rock Engineering* (1995).

[45] J. W. Rudnicki, Geomechanics, Int. J. Solids and Structure **37**, 349 (2000).

[46] B. Utter and R. P. Behringer, Transients in sheard granular matter, Euro. Phys. J. E. **14**, 373 (2004).

[47] Y. Ban, X. Fu, Q. Xie, and J. Duan, Time-sensitivity mechanism of rock stress memory properties under tensile stress, J. Rock Mech. Geotech. Eng. **12**, 528 (2020).

[48] T. Brunet, X. Jia, and P. Mills, Mechanisms for acoustic absorption in dry and weakly wet granular media, Phys. Rev. Lett. **101**, 138001 (2008).

[49] C. G. Sammis and M. G. Bostock, A granular jamming model for low-frequency earthquakes, J. Geophys. Res.: Solid Earth **126**, B021963 (2021).

[50] E. Somfai, J.-N. Roux, J. H. Snoeijer, M. van Hecke, and W. van Sarloos, Elastic wave propagation in confined granular systems, Phys. Rev. E **72**, 021301 (2005).